



Purification of Disc-Shaped Diatoms from the Southern Ocean Sediment by a Cell Sorter to Obtain an Accurate Oxygen Isotope Record

Ijiri, Akira ; Izumi, Takeshi ; Morono, Yuki ; Kato, Yuji ; Terada, Takeshi ; Ikehara, Minoru

(Citation)

ACS Earth and Space Chemistry, 5(10):2792-2806

(Issue Date)

2021-09-03

(Resource Type)

journal article

(Version)

Accepted Manuscript

(Rights)

© 2021 American Chemical Society

This document is the Accepted Manuscript version of a Published Work that appeared in final form in ACS Earth and Space Chemistry, copyright © 2021 American Chemical Society after peer review and technical editing by the publisher. To access the fina...

(URL)

<https://hdl.handle.net/20.500.14094/0100476799>



Purification of disc-shaped diatoms from Southern Ocean sediment by cell sorter to obtain accurate oxygen isotope record

Akira Ijiri^{1,2}, Takeshi Izumi³, Yuki Morono¹, Yuji Kato⁴, Takeshi Terada⁵, Minoru Ikehara^{3,4}*

¹ Kochi Institute for Core Sample Research (KOCHII), Institute for Extra-cutting-edge Science and Technology Avant-garde Research (X-Star), Japan Agency for Marine-Earth Science and Technology (JAMSTEC), B200 Monobe, Nankoku, Kochi 783-8502, Japan

² Graduate School of Maritime Sciences, Kobe University, 5-1-1 Fukaeminamimachi, Higashinada-ku, Kobe 658-0022, Japan

³ Graduate School of Integrated Arts and Sciences, Kochi University, 2-5-1 Akebono-cho, Kochi 780-8520, Japan

⁴ Center for Advanced Marine Core Research, Kochi University, B200 Monobe, Nankoku, Kochi 783-8502, Japan

⁵ Marine Works Japan Ltd., 3-54-1 Oppamahigashimachi, Yokosuka 237-0063, Japan

*Tel: +81-78-431-6242

Email: ijiri@maritime.kobe-u.ac.jp

KEYWORDS

disc-shaped diatom; cell sorter; oxygen isotope; Southern Ocean; Conrad Rise; sediment core

ABSTRACT

The oxygen isotopic composition ($\delta^{18}\text{O}$) of diatom frustules is potentially a quantitative paleoenvironmental proxy. However, the $\delta^{18}\text{O}$ analysis has some uncertainties because of difficulties in removing clay-mineral contamination and taxon-specific separation, due to the small size of diatom frustules. The clay-mineral contamination seriously affects $\delta^{18}\text{O}$ measurements, and the $\delta^{18}\text{O}$ of bulk diatoms contains a mixture of information from diatoms living in various seasons and water depths. To resolve such problems, we established a new method to purify the frustules of disc-shaped diatoms using cell sorter, and succeeded in removing the clay-mineral contamination and restricting the number of species for the $\delta^{18}\text{O}$ analysis. We developed this method using samples from a sediment core retrieved from the Conrad Rise in the Indian Ocean sector of the Southern Ocean. First, the disc-shaped diatoms were enriched and cleaned by sieving, elutriation, and heavy-liquid separation. The samples were then further purified by cell sorter. Regardless of the diatom assemblage or the sediment type in the core sample, this method generated samples consisting of more than 95% disc-shaped diatoms, dominated by *Thalassiosira lentiginosa* (Janisch) Fryxell, which occurs ubiquitously throughout the Southern Ocean. The $\delta^{18}\text{O}$ profile for the sediment core obtained from purified disc-shaped diatoms showed the last glacial cycle since ca. 40 ka, which can be correlated with the LR04 benthic $\delta^{18}\text{O}$ stack record, and the temperature record in the EPICA Dome C ice core,

indicating that this method can contribute to obtaining an accurate $\delta^{18}\text{O}$ record of diatoms associated with glacial–interglacial cycles.

1. INTRODUCTION

The oxygen isotopic composition ($\delta^{18}\text{O}$) of foraminiferal shells (made of calcium carbonate, CaCO_3) is a fundamental quantitative proxy in paleoceanography, because this $\delta^{18}\text{O}$ reflects the temperature-dependent oxygen isotopic fractionation between seawater and carbonates.¹⁻³ Carbonate microfossils such as foraminiferal shells, however, are not preserved in deep-sea sediment below the calcium carbonate compensation depth, and foraminiferal production is limited in the polar oceans. Instead, the polar oceans, including the Southern Ocean, contain siliceous sediments with abundant fossil diatoms instead of foraminifera-bearing calcareous sediments.⁴ Even though the Southern Ocean plays an important role in global climate change, the lack of $\delta^{18}\text{O}$ information makes quantitative studies of the paleoceanography of the Southern Ocean difficult.⁵⁻⁷

The $\delta^{18}\text{O}$ of diatom frustules, which are composed of biogenic opal, would be an alternative quantitative proxy to foraminiferal $\delta^{18}\text{O}$. Indeed, several studies have demonstrated the potential for $\delta^{18}\text{O}$ of diatom frustules as a paleoenvironmental proxy reflecting the water temperature and $\delta^{18}\text{O}$ of seawater.⁸⁻¹⁵ However, there is some uncertainty associated with the $\delta^{18}\text{O}$ of diatoms as a paleoceanographic proxy because of many remaining difficulties in the analytical procedures. In particular, there is no established reliable method for pretreatment of samples. Because of the small size of diatom valves (several tens of μm), it is not possible to manually isolate any morphological taxon under a stereomicroscope, as is possible with foraminifera. Therefore, in most previous studies, measurement of diatom $\delta^{18}\text{O}$ has been carried out on samples that included some clay minerals and several diatom species. Thus far, removal of clay-mineral contamination and separation of diatom frustules by species for taxon-specific $\delta^{18}\text{O}$ measurements have persisted as challenges awaiting solutions.¹⁵

Because clay minerals generally have $\delta^{18}\text{O}$ values $>20\text{‰}$ lower than those of diatoms, sample contamination by clay minerals seriously affects $\delta^{18}\text{O}$ measurements.¹⁶ Clay minerals can be removed by using the “heavy-liquid separation method”, by utilizing the difference of specific gravity of clay minerals and diatom frustules.¹⁶ In addition, diatoms can be separated from contaminants using gravitational split-flow thin fractionation, which separates particles of different densities in a laminar flow.^{17–19} Recently, a new method for rapid extraction of diatom frustules from lacustrine sediment using flow cytometry was reported.²⁰ The principles of flow cytometry are explained in more detail later in the Method section.

The previous $\delta^{18}\text{O}$ analyses of different size fractions of diatom frustules indicate that there may be species or size-related effects in the $\delta^{18}\text{O}$ of bulk diatoms, i.e., the differences in production season and/or water depth of each species or vital effect.^{21,22} Diatoms have two distinct shapes: centric diatoms are radially symmetric, whereas pennate diatoms are broadly bilaterally symmetric. Recently, Studer et al.²³ enriched samples with each of these two types by elutriation, in which hydrodynamically “heavier” centric diatoms settle faster than pennate. They analyzed the nitrogen isotopic composition of the organic matter bound to the diatom valves in the pennate-rich and centric-rich diatom assemblages and reported that these assemblages likely record different nutrient information reflecting habitat water-depth and production season. Even with only a rough separation of these two types of diatom, their respective $\delta^{18}\text{O}$ values could provide useful information about past changes in temperature and salinity at different seasons and water depths. In other words, restricting the number of species for $\delta^{18}\text{O}$ analysis is essential for obtaining more accurate information and avoiding mixed information from various seasons and water temperatures.

In this study, we developed a new purification method for “disc-shaped” diatoms by using flow cytometry in the form of a cell sorter (hereafter, cell sorter). The cell sorter can sort microparticles on the basis of optical characteristic of the subject, such as size, internal structure, fluorescence intensity or wavelength, at high speed (tens’ thousands particles per second in the instrument that we use), and is used for the analysis or selective sorting of cells. Recently, this technique has been applied to the separation of microbes, micro-manganese nodules, and diatom frustules from sediment samples.^{20,24,25} The aim of this study was to obtain accurate, taxon-specific $\delta^{18}\text{O}$ records that can be applied to the various oceanographic settings in the Southern Ocean. We therefore targeted *Thalassiosira lentiginosa* (Janisch) Fryxell, which is distributed ubiquitously throughout the Southern Ocean, especially in permanent open-ocean zones.²⁶ *T. lentiginosa* is the most dominant species of disc-shaped diatom in the Southern Ocean, so the purification of disc-shaped diatoms from Southern-Ocean sediments means the enrichment of *T. lentiginosa*. In addition, this taxon has a long stratigraphic range from approximately 4.2 Ma to the present.²⁷ Hence, measuring the $\delta^{18}\text{O}$ of this taxon would contribute substantially to the reconstruction of paleoceanographic changes in the Southern Ocean over several glacial-interglacial cycles. Note that “disc-shaped” diatoms are included within the centric diatoms. Because centric diatoms are defined as radially symmetric, they include species that are not disc-shaped, such as *Eucampia antarctica* (Castracane) Mangin, which is also a ubiquitous taxon in the Southern Ocean.²⁸ Purification of only disc-shaped diatoms would allow for high-purity enrichment of *T. lentiginosa*.

Our purification method for disc-shaped diatoms can be applied not only for $\delta^{18}\text{O}$ analysis but also for other chemical and isotopic analyses. In particular, the method can be directly applied to the diatom silicon isotope composition ($\delta^{30}\text{Si}$), which is a proxy for local silicic acid

utilization.^{29–32} In addition, the method would be applicable to analyses of the carbon and nitrogen isotopic compositions ($\delta^{13}\text{C}$ and $\delta^{15}\text{N}$) of organic matter occluded within diatom frustule walls, which are used as a proxy for the carbon and nitrogen cycles at the sea surface.^{23,33–36}

2. MATERIALS AND METHODS

2.1. Materials

In this study we used sediment core COR-1bPC, retrieved from the southwestern slope of the Conrad Rise in the Indian Ocean sector of the Southern Ocean (54°16'S, 39°46'E; water depth, 2828 m; core length, 10.5 m) in 2010 during cruise KH-10-7 of R/V *Hakuho Maru* (Figure 1a).³⁷ The Conrad Rise is a relatively shallow feature (<3000 m depth), lying within the southern core of the Antarctic Circumpolar Current (ACC). The ACC bifurcates on the western side of the Conrad Rise, forming jets along the 3500 m isobaths to the north and south and converging again on its eastern side.³⁸ Core COR-1bPC is composed of diatom ooze. The sediments in the upper approx. 4 m are milky-white and consist of many siliceous microfossils, whereas the lower approx. 4 m is greenish-gray and contains clay minerals in addition to siliceous microfossils (Figure 1b). The lightness (L^*) values are relatively dark from the base of the core to 4.7 m depth, above which they change to lighter values (Figure 1c). The correlation between L^* and the temperature record estimated from the hydrogen isotopic composition (δD) in the EPICA Dome C ice core (Figure 1) suggests that the increase in the L^* color reflectance curve of core COR-1bPC from 4.7 m corresponds to the temperature increase in the ice core, which represents the onset of deglaciation at 17.4 ka.^{37,39} Based on this correlation and ^{14}C -dating of planktonic foraminifera,³⁷ we estimate that the sediments in the core were deposited from 42 ka (middle Marine Isotope Stage [MIS] 3) to the present.

Core COR-1bPC was cut into meter-long section and then opened with a cutter and sub-sampled for analysis of paleoenvironmental proxies. After the sub-sampling was complete, the residual sediments contacted with the inside of core liner were scraped together and combined by section. For the basic experiment to develop the purification method described below, we used the combined residual sediment from Sections 4 (151–248 cm), 8 (550–649 cm), and 11 (851–949 cm), corresponding to 7.3–11.4 ka (MIS 1), 19.7–24.1 ka (MIS 2), and 33.1–37.5 ka (MIS 3), respectively (Figure 1a), because we needed a large amount of sample material for development of the method. After we established the method, we used the method to analyze the $\delta^{18}\text{O}$ of disc-shaped diatoms throughout core COR-1bPC. Sediment samples for this $\delta^{18}\text{O}$ analysis were collected from the core at 50 to 100 cm intervals and 2 cm widths.

Fig. 1

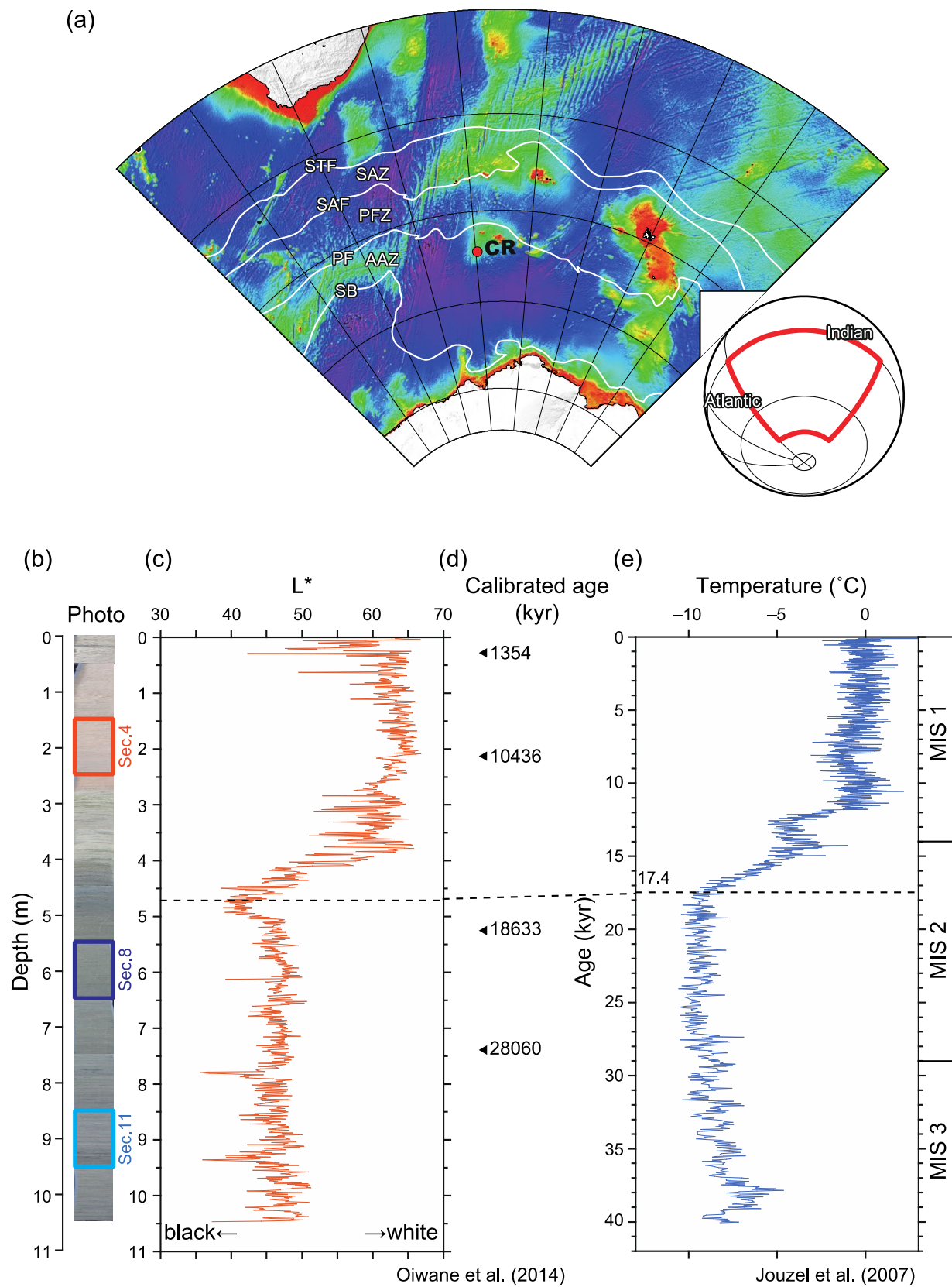


Figure 1. Map showing the coring site, and descriptions of core COR-1bPC. (a) Map of the Indian sector of the Southern Ocean, (b) photograph of the core, (c) L^* (lightness), (d) calibrated age of core COR-1bPC, and (e) the temperature profile from the EPICA Dome C ice core. In (a) the red circle indicates the coring site for COR-1BC. CR: Conrad Rise. Oceanic fronts are shown in white lines. STF: Subtropical Front, SAF: Subantarctic Front, PF: Polar Front, SB: Southern Boundary of ACC. Oceanic zones are also indicated. SAZ: Subantarctic Zone, PFZ: Polar Front Zone, AAZ: Antarctic Zone. The dotted line connecting (c–e) shows an age tie point between core COR-1bPC (4.7 m) and the EPICA Dome C ice core (17.4 ka). The horizontal bars on the right side of (e) indicate the boundaries between MIS 1, MIS 2, and MIS 3. This figure is reproduced from Oiwane et al. with the permission of the copyright holder (Elsevier)(License number: 5131090217162).³⁷

2.2. Pretreatment of core samples

Before purifying disc-shaped diatoms by cell sorter, it was necessary to include pre-enrichment process to enrich the disc-shaped diatoms to avoid potential noises hampering selective sorting of disc-shaped diatom frustules. To reduce contaminants and enrich the disc-shaped diatoms, we performed a pretreatment that combines the “heavy-liquid separation method” and the “elutriation method”.^{16,23} The three pretreatment steps were as follows (Figure 2).

Step 1: Removal of organic matter and carbonates, and sieving of the sample (modified from Swann et al.¹⁴)

Organic matter in sediment samples was decomposed using H_2O_2 . Approximately 6 g of wet sediment and 40 mL of 30% H_2O_2 were introduced into a 50 mL polypropylene conical centrifuge tube. The tube was placed in a constant-temperature bath at 70 °C for 6 h, and shaken every hour using a vortex mixer. The treated samples were centrifuged at 2500 rpm for 10 min. After that, the supernatant was removed. The sample was washed with Milli-Q water to remove H_2O_2 . For this, 50 mL of Milli-Q water was added to the tube. The samples were centrifuged at 2500 rpm for 10 min, again, and the supernatant was then removed. The centrifugation and removal of the supernatant were repeated about five times. To check for complete removal of H_2O_2 , we confirmed that the electrical conductivity of the supernatant was less than 100 $\mu\text{S}/\text{cm}$, i.e., less than that of tap water (200 $\mu\text{S}/\text{cm}$), by using an electrical conductivity meter (LAQUAtwin EC-33B, Horiba, Ltd., Kyoto, Japan). In the following procedures, the washing procedure for removing chemicals using Milli-Q water is the same as that described here for removal of H_2O_2 .

To dissolve carbonate, the sample was acidified by adding 40 mL of 5% HCl to the 50 mL centrifuge tube containing the sample. The tube was shaken with a vortex mixer and placed at room temperature for 12 h. The sample was then washed with Milli-Q water to remove HCl.

The samples were sieved to obtain the 20–32 μm fractions by using 63, 45, 32, and 20 μm stainless-steel cloth. The fraction-size of 20–32 μm was selected to avoid stuck of particles at the nozzle of the cell sorter of which the diameter was 100 μm . Because the mean diameter of *T. lentiginosa*, that is our target, in the Southern Ocean reportedly varies between 43.2 and 57.3 μm , we cannot collect the overall *T. lentiginosa* assemblage. Instead, the valve area of *T. lentiginosa* in the sea-ice zone varies between 400 and 1200 μm^2 , equal to a diameter of 23–39 μm .⁴⁰ Therefore, we expected that diatom frustules in the 20–32 μm size fraction would include abundant *T. lentiginosa* associated with sea ice. Furthermore, the analysis of limited size fraction can minimize the difference in $\delta^{18}\text{O}$ signal between growth phases.^{21,22} A sieve was placed on a tall 500 mL beaker, and a sample was poured onto the sieve with Milli-Q water. Water was added and the sieve was shaken by hand until the liquid passing through the sieve was no longer turbid. A total of 4 L of Milli-Q water was used for the sieving of each sample.

Step 2: Removal of detritus and enrichment of disc-shaped diatoms (modified from Studer et al.²³)

To remove detrital particles attached to diatom frustules, such as small clay-mineral particles and diatom debris, and enrich the disc-shaped diatoms, we used ultrasonication and elutriation. Ultrasonication was used to disperse the diatom frustules and detrital particles such as diatom fragments attached to the frustules (Supplemental Figure S1). Then, by using gentle centrifugation, the disc-shaped diatoms accumulated at the bottom of the tube, while the pennate

diatoms remained in the supernatant.²³ In our procedure, detrital particles also remained in the supernatant.

A sample of the 20–32 μm fraction and 50 mL of Milli-Q water were introduced into a 50 mL centrifuge tube. The sample was suspended using a vortex mixer then ultrasonically dispersed with a 50 kHz ultrasonic cleaner for 1 min. The sample was re-suspended with a vortex mixer, and centrifuged at 1000 rpm for 1 min. After the centrifugation, the supernatant (containing pennate diatoms and detrital particles) was immediately removed, leaving the precipitate, which was enriched in disc-shaped diatoms. The ultrasonication and elutriation were repeated three times.

Step 3: Removal of clay minerals (modified from Morley et al.¹⁶)

To remove the clay minerals, we used heavy-liquid separation with sodium polytungstate (SPT; $3\text{Na}_2\text{WO}_4 \cdot 9\text{WO}_3 \cdot \text{H}_2\text{O}$).¹⁶ The heavy liquid was prepared by dissolving sodium polytungstate in Milli-Q water (2.1 g/mL). Any suspended matter in the prepared heavy liquid was removed using a 20 μm -mesh sieve.⁴¹ A 50 mL centrifuge tube containing the enriched disc-shaped diatoms was filled with 30 mL of SPT solution, suspended using a vortex mixer, and centrifuged at 2500 rpm for 20 min. The supernatant enriched in disc-shaped diatoms was immediately removed and introduced into another 50 mL centrifuge tube. The collected supernatant was washed with Milli-Q water to remove the heavy liquid. The extracted sample enriched in disc-shaped diatoms was sieved again through 20 and 32 μm mesh to remove any large particles that might have become stuck in the flow-path of the cell sorter. The precipitate from the separation was also washed with Milli-Q water to remove the heavy liquid and stored in another vial for later $\delta^{18}\text{O}$ analysis.

We performed the pretreatment using eight samples per batch. Total time required for one batch was 5 days (1 day for H₂O₂ treatment, 1 day for HCl treatment, 2 days for sieving, 0.5 days for sonication and elutriation, and 0.5 days for STP separation and sieving).

Fig .2

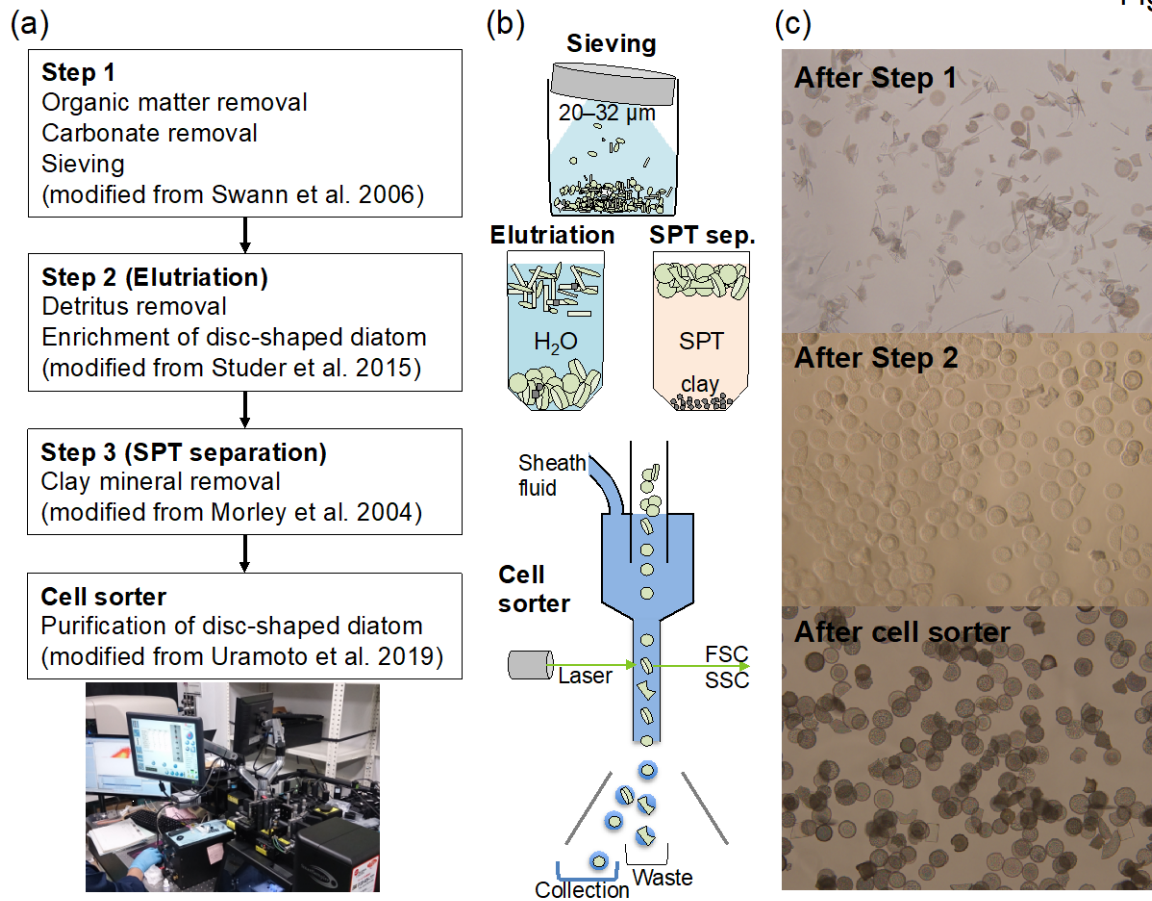


Figure 2. Procedure for the purification of disc-shaped diatoms from sediment samples. (a) Flow-chart of the procedure, (b) a schematic showing each treatment, and (c) representative photographs of the treated samples after each step.

2.3. Cell sorter

We selectively sorted the disc-shaped diatoms by using a Moflo XDP cell sorter (Beckman Coulter, Brea, CA, USA). The cell sorter uses a sheath fluid to hydrodynamically focus a sample suspension through a small nozzle (Figure 2). The tiny stream of fluid carries the subject particles one at a time past a laser. Light scattered from the subjected cells or particles is detected as they pass through the laser beam. A detector in front of the laser beam measures forward scatter (FSC) and several detectors to the side measure side scatter (SSC) and fluorescence. Specific ranges of values can be selected for the optical data, and particles that fall within these ranges are sorted away from the sample stream and collected, leaving the unwanted detritus to be routed to waste.

For the sheath fluid we used a solution of 1% NaCl in Milli-Q water. The enriched disc-shaped diatom sample was suspended in SPT solution (1.1 g/mL) and introduced into the cell sorter. The disc-shaped diatom frustules were sorted into an antistatic balance dish (44 × 44 × 8 mm; BIO-BIK, INA OPTIKA CO., LTD, Osaka, Japan). The collected sample was washed with Milli-Q water. Five repeated washings brought the electrical conductivity of the supernatant to 0 μS/cm. Zero μS/cm of the electrical conductivity suggests that almost all of tungstate were removed during the sorting and the washing.

2.4. Analytical methods

The oxygen isotopic composition ($\delta^{18}\text{O}$) of diatom silica was analyzed by an online analytical system, using the inductive high-temperature carbon reduction (iHTR) method,⁴² coupled to a continuous-flow isotope ratio mass spectrometry system (CF-IRMS) (Thermo Finnigan

DELTA^{plus} Advantage) with an open-split interface (Thermo Finnigan ConFlo III) as described by Ijiri et al.⁴³ This analytical system allows for the $\delta^{18}\text{O}$ analysis of the sub-milligram diatom samples, which is essential for the analysis of small amounts of samples purified by the cell sorter.⁴³ In the iHTR method, the weakly bonded outer hydrous layers of biogenic opal are volatilized stepwise at high temperature (1100 °C) under high vacuum. After complete dehydration, the temperature is raised to 1600 °C to reduce silica and produce carbon monoxide (CO). The $\delta^{18}\text{O}$ of the CO is then determined by CF-IRMS. For the analysis, approximately 200 µg of sample and 2000 µg of glassy carbon were mixed and introduced into the analytical system. The standard deviation obtained from the analyses of laboratory standard (synthetically produced amorphous silica, NFC⁴⁴) was <0.5‰.

After each pretreatment step the samples were observed by Scanning Electron Microscope (SEM; JSM-6500F, JEOL, Japan) and subjected to Energy-dispersive X-ray spectroscopy (EDS; JED-2300, JEOL, Japan) analysis. Prior to the analysis, the specimens were attached to carbon tapes and coated with platinum. Following Maier et al.,³² the elemental composition was acquired through integration of X-ray intensities determined from an area of about $250 \times 350 \mu\text{m}$. EDS results are expressed as weight percentages of oxides, normalized to 100 wt.%. We conducted triplicate analyses in different areas for each sample and used the mean value to determine the elemental composition.

The contamination percentage (“clay-mineral percentage”) was calculated from the Al_2O_3 composition of a given sample and of the end-member “clay mineral” (100% contaminant, no biogenic silica), with Al_2O_3 being regarded as a tracer of clay minerals, using the following equation:

$$\%contam = (Al_2O_{3sample}/Al_2O_{3contam}) \times 100 \quad (1)$$

where %contam represents the percentage of contamination in the sample, and $Al_2O_{3sample}$ and $Al_2O_{3contam}$ represent the percentages of Al_2O_3 in the sample and in the 100% contamination end-member.^{15,45–46} For $Al_2O_{3contam}$, we used the mean value of 15.4 wt.% ($n = 15$) obtained from point analyses of three clay minerals in the MIS 3 sample.

Based on mass-balance calculations, the measured $\delta^{18}O$ value was corrected for the contamination percentage using the following equation:

$$\delta^{18}O_{corr} = (\delta^{18}O_{measured} - \%contam \times \delta^{18}O_{contam})/\%purity \quad (2)$$

where $\delta^{18}O_{corr}$, $\delta^{18}O_{measured}$, and $\delta^{18}O_{contam}$ are the $\delta^{18}O$ value corrected for the contamination, the measured $\delta^{18}O$ value, and the $\delta^{18}O$ value of the contaminants, respectively.¹⁵ The parameter %purity is the degree of purity ($100\% - \%contam$) of the sample. Because the $\delta^{18}O$ of the clay minerals is unknown, we used +20‰ for $\delta^{18}O_{contam}$, which is around the mean value of the previously reported $\delta^{18}O$ of marine clay, ranging from +13‰ to +29‰ (Vienna Standard Mean Ocean Water, VSMOW).^{47,48}

Diatom assemblages were analyzed after elutriation for enrichment of disc-shaped diatoms and after cell sorter-purification of disc-shaped diatoms to verify how disc-shaped diatoms were enriched/purified. Microslides for the diatom analyses were prepared using a 24 x 40 mm² cover glass and photocuring adhesive. All diatoms were identified and counted at the species level until 50–100 individual valves were counted for one slide. A single centric diatom valve was counted as one when more than half of the valve was observed. Broken specimens of pennate diatoms

were counted as one valve when two apices were observed. These observations were made under a light microscope at 400–1000× magnification.

3. RESULTS AND DISCUSSION

3.1. Contamination in pretreated samples

We evaluated the amount of clay and other siliceous minerals contamination in the samples, and its influence on the $\delta^{18}\text{O}$ of the diatoms during the pretreatment Step 1 (chemical cleaning and sieving), Step 1+3 (no elutriation but SPT separation), and Step 1+2+3 (complete pretreatment) with the MIS 1 and MIS 3 samples.

On the basis of the SEM observations, we confirmed that the diatom frustules were enriched through the sieving treatment (Step 1) and the SPT separation (Steps 1+3) for both MIS 1 and MIS 3 samples (Figure 3). The EDS analysis of MIS 1 and MIS 3 samples showed an increase of SiO_2 content and decrease of Al_2O_3 content in the order of pretreatment Step 1, Steps 1+3, and Steps 1+2+3 (Figure 4; Supplemental Table S1). There was no Al_2O_3 detected in the detrital particles that settled during the SPT separation from the MIS 1 sample; in the MIS 3 sample the Al_2O_3 content was 4.9 wt.%.

The average $\delta^{18}\text{O}$ values after each pretreatment step for the MIS 1 sample were +42.6‰, +43.2‰, and +40.1‰ at Step 1, Steps 1+3, and Steps 1+2+3, respectively (Figure 4a, Supplemental Table S2); that of the detrital particles was +43.5‰. The average $\delta^{18}\text{O}$ values of the MIS 3 sample were +36.0‰, +42.7‰, and +41.8‰ at Step 1, Steps 1+3, and Steps 1+2+3, respectively (Figure 4b, Supplemental Table S2); that of the detrital particles was +20.2‰. Only

when comparing the samples treated with Steps 1+2+3, MIS 1 have lower $\delta^{18}\text{O}$ values than MIS 3, which is the generally accepted environmental variability, i.e., MIS 1 was warmer than MIS 3.

In the MIS 3 sample, the detrital particles enriched in clay or siliceous minerals had the lowest $\delta^{18}\text{O}$ value and the highest Al_2O_3 content, indicating that the origin of the contamination was clay minerals as previously reported.^{15,32,45,46} (Figures 4b, 4f). The lowest Al_2O_3 content was observed after Steps 1+2+3, suggesting that elutriation for enrichment of disc-shaped diatoms can remove clay minerals. Despite having the lowest Al_2O_3 content, indicating the least contamination by clay-minerals, the disc-shaped diatoms enriched by Steps 1+2+3 had a $\delta^{18}\text{O}$ value 0.9‰ lower than that of bulk diatoms treated with Steps 1+3 (Figure 4b). This result suggests that the $\delta^{18}\text{O}$ of disc-shaped diatoms is lower than that of other diatoms. Based on the Al_2O_3 content (0.1 wt.%), the clay-mineral contamination was estimated at 0.6‰ for the disc-shaped diatom-rich sample from MIS 3. Assuming that the end-member $\delta^{18}\text{O}$ of clay minerals is +20‰, the offset of the $\delta^{18}\text{O}$ corrected for the contamination (+41.9‰) from the measured value (+41.8‰) was 0.1‰.

We also conducted EDS analysis on the disc-shaped-diatom-enriched MIS 2 sample because this sample could have contained more clay minerals originated from aeolian dust and/or ice-rafted debris than the MIS 3 sample.^{5,7} The Al_2O_3 content of the MIS 2 sample was 0.3 wt.% (Supplemental Table S1), and the clay-mineral contamination was estimated to be 1.8‰. The offset of the corrected $\delta^{18}\text{O}$ for the contamination (+41.5‰) from the measured value (+41.1‰) was 0.4‰.

In contrast to the MIS 3 sample, the $\delta^{18}\text{O}$ value of the detrital particles from the MIS 1 sample was the highest, and that of the disc-shaped diatoms enriched by Steps 1+2+3 was the lowest (Figure 4a, Supplemental Table S2). The Al_2O_3 contents in the MIS 1 samples were lower than

in MIS 3 samples. The percentage of clay-mineral contamination of the MIS 1 sample after Steps 1+2+3 was 0.04%. This result indicates that clay-mineral contamination was not significant in the MIS 1 sample, but other contaminants potentially increased the $\delta^{18}\text{O}$ value. It is a possibility that the $\delta^{18}\text{O}$ of other siliceous microfossils observed in the detrital particles, such as silicoflagellates (Figure 3g), was higher than that of diatoms. The removal of these other siliceous microfossils would have contributed to the result of the Steps 1+2+3 treated sample that was rich in disc-shaped diatoms and showed a lower $\delta^{18}\text{O}$ value (by 3.1‰) than the bulk diatom sample treated in Steps 1+3. Another possibility is that the $\delta^{18}\text{O}$ value of disc-shaped diatoms is lower than that of pennate diatoms as was the case in MIS 3.

These results indicate that Steps 1+2+3, including enrichment of disc-shaped diatoms, is important to eliminate the contaminants. The evaluation of the contamination showed the relatively insignificant clay-mineral contamination of the MIS 1 sample, and the reduced effect of clay-mineral contamination for the MIS 2 and MIS 3 samples resulting from pretreatment with Steps 1+2+3. The offset of the corrected $\delta^{18}\text{O}$ for the contamination from the measured value was <0.4‰, which is smaller than the analytical error for our analytical system (<0.5‰). We, therefore, did not correct the measured $\delta^{18}\text{O}$ values for clay-mineral contamination in the subsequent section of this study.

Fig. 3

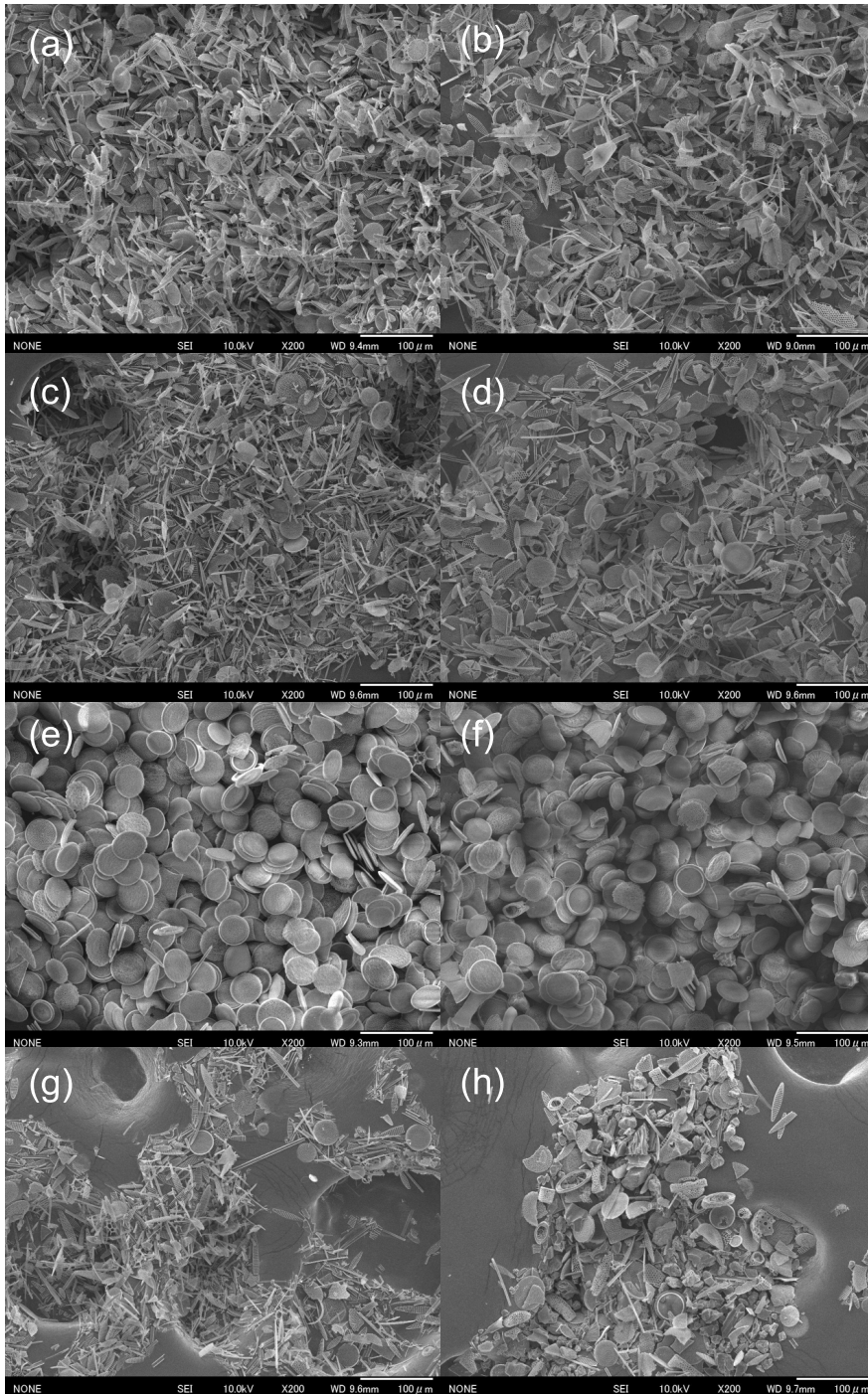


Figure 3. SEM images of the pretreated samples from MIS 1 and MIS 3. Samples treated by Step 1: (a) MIS 1 and (b) MIS 3; treated by Steps 1+3: (c) MIS 1 and (d) MIS 3; treated by Steps 1+2+3: (e) MIS 1 and (f) MIS 3; and the settled detrital particles from the SPT solution in Steps 1+3: (g) MIS 1 and (h) MIS 3.

Fig. 4

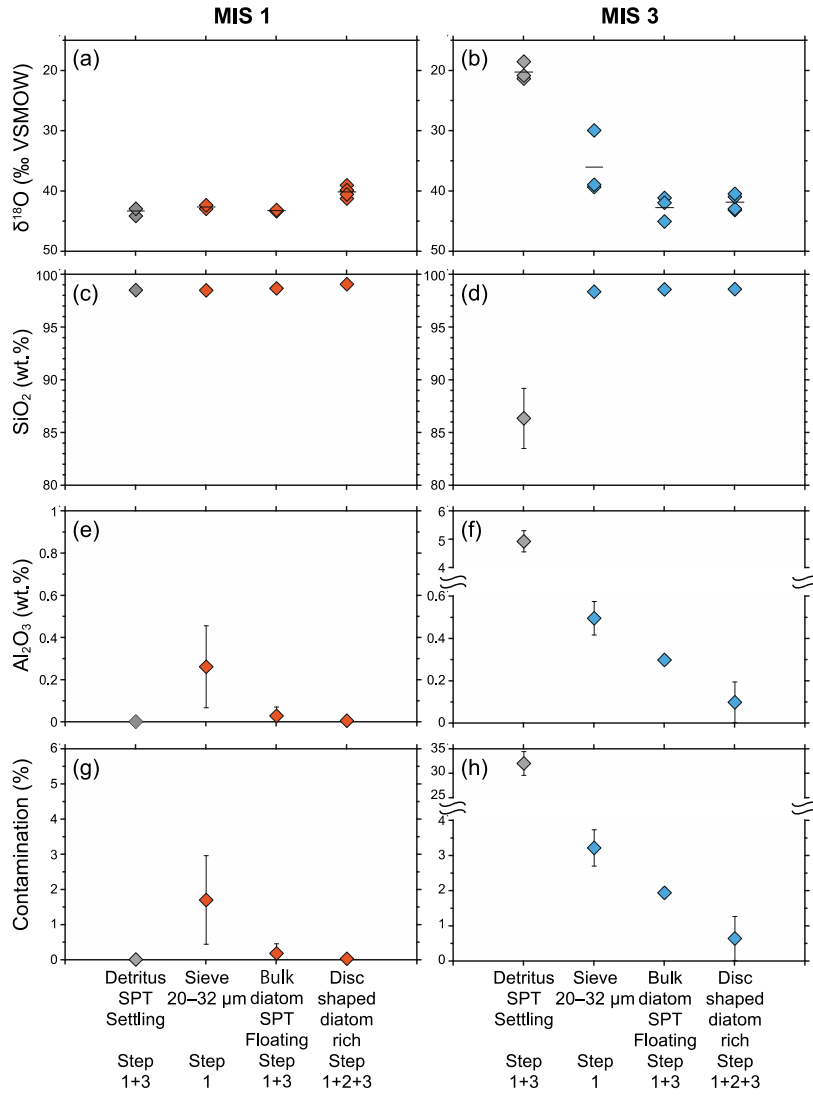


Figure 4. Measured $\delta^{18}\text{O}$ values and elemental compositions of samples at each pretreatment step, i.e., detrital particles that settle in the SPT solution during Steps 1+3, the 20–32 μm sieved fraction from Step 1, the bulk diatoms that float in the SPT solution during Steps 1+3, and the disc-shaped diatoms enriched by elutriation during Steps 1+2+3. Measured $\delta^{18}\text{O}$ values of samples for (a) MIS 1 and (b) MIS 3, SiO_2 contents for (c) MIS 1 and (d) MIS 3, Al_2O_3 contents for (e) MIS 1 and (f) MIS 3, and percentage of clay-mineral contamination as estimated from Al_2O_3 content for (g) MIS 1 and (h) MIS 3.

3.2. Enrichment of disc-shaped diatoms by elutriation for the MIS1, 2, and 3 samples

Once the pretreatment steps were completed for the MIS 1 and MIS 3 samples, the MIS 2 sample was also pretreated and analyzed for $\delta^{18}\text{O}$, but we did not perform detailed observations after each pretreatment step. From about 6 g of initial wet sediment sample, we collected about 20 mg of disc-shaped diatom rich sample by the pretreatment.

The percentages of disc-shape diatoms in samples enriched by Steps 1+2+3 were 100%, 87%, and 87% for MIS 1, MIS 2, and MIS 3, respectively (Figure 5b, Supplemental Table S3). The dominant species other than disc-shaped diatoms in MIS 2 and MIS 3 was *Eucampia antarctica* (MIS 2, 12%; MIS 3, 10%) which is centric, but not disc-shaped.

The $\delta^{18}\text{O}$ values of disc-shaped diatoms enriched by Steps 1+2+3 for MIS 1, 2, and 3 were $+40.1\text{‰} \pm 0.7\text{‰}$ (1σ ; $n = 5$), $+41.1\text{‰} \pm 0.6\text{‰}$ ($n = 6$), and $+41.8\text{‰} \pm 1.2\text{‰}$ ($n = 4$), respectively (Figure 5a). The average value of $\delta^{18}\text{O}$ at MIS 1 is 1‰ lower than that at MIS 2, suggesting a lower $\delta^{18}\text{O}$ and higher temperature of seawater at MIS 1 than at MIS 2, and consistent with the environmental change from MIS 2 to MIS 1. However, $\delta^{18}\text{O}$ varied more than 2‰ within each sample. The large variation suggests that the pretreatment for the enrichment of disc-shaped diatoms is not enough to obtain accurate $\delta^{18}\text{O}$ records.

3.3. Purification of disc-shaped diatoms by cell sorter for the MIS1, 2, and 3 samples

We further purified the cleaned and enriched disc-shaped diatoms from the MIS 1–3 samples by cell sorter. We then analyzed the $\delta^{18}\text{O}$ of the purified samples and compared the values to those of the samples enriched in disc-shaped diatoms by pretreatment.

Cell sorter utilizes the optical characteristics of particles not only fluorescence but also forward scatter (FSC) and side scatter (SSC).^{20,25} FSC is the light signal detected along the path of the

laser, and SSC is the signal detected at a ninety-degree angle relative to the laser. The measurement of FSC allows for the discrimination of particles by size. FSC is primarily caused by light diffraction around the particles. The interface between laser and particles causes the light to refract or reflect, which is the source of SSC signal. Complex structure of diatoms should be reflected in the wide range of SSC signals.

Figure 6a–c and Figure 6d–f show representative cytograms of the disc-shaped-diatom-rich samples from MIS 1 and MIS 3, respectively. Initial attempts of sorting and following observation of sorted particles allowed us to identify areas of the diatom frustules (areas enclosed by dashed lines in Figure 6a and d) in plots of FSC and SSC heights. However, further sorting revealed that the area also contained fragments of diatoms, and other diatoms such as *Eucampia antarctica* or pennate diatoms (Figure 6g). Then, we conducted many cycles of sorting and observation for fine-tuning the sorting area and achieved a greater purity of disc-shaped diatoms by selecting the areas enclosed by the solid lines (SSC: 6.6×10^2 – 2.1×10^4 ; FSC: 2.1×10^3 – 4.8×10^3) in Figure 6a and d. Note that the parameters vary depending on the device, optical alignments, and settings of detectors. In the FSC and SSC histograms of the MIS 1 sample, the particle counts showed a peak at the area of disc-shaped diatoms (Figure 6b, c). However, in the MIS 3 sample, although there was no recognizable peak for disc-shaped diatoms because of the high counts of other particles (Figure 6e, f), we were able to sort disc-shaped diatoms in high purity like the MIS 1 sample (Figure 6h).

At optimized conditions, the sorting rate was around 100 particles per second, and we could collect about 5×10^5 particles of disc-shaped-diatom frustules (more than 200 μg) from each sample in about 90 min. The solution for the sorting was adjusted to about 400 μg of disc-shaped diatom rich samples per mL of SPT solution. The collection of 5×10^5 disc-shaped-diatom

particles required about 1 mg (dry weight) of the disc-shaped-diatom-rich samples treated by Steps 1+2+3, i.e. 2.5 mL of the solution.

The percentages of disc-shaped diatoms in the samples purified by cell sorter were 98%, 98%, and 99% for MIS 1, 2, and 3, respectively (Figure 5b, Supplemental Table S3), indicating that the purification was successful. The MIS 1 sample was dominated by *T. lentiginosa* (58%) followed by *Azpeitia tabularis* (Grunow) Fryxell et Sims (25%), and *Thalassiosira oliverana* (O'Meara) Makarova et Nikolaev (17%). The MIS 2 and MIS 3 samples were entirely dominated by *T. lentiginosa* (90% and 95%, respectively), followed by *T. oliverana* as a minor species. It is worth noting that *E. antarctica*, which was present in the MIS 2 and MIS 3 samples after pretreatment by Steps 1+2+3, was mostly removed by cell sorter, and *T. lentiginosa*, which was our target, was enriched (Figure 5b).

The $\delta^{18}\text{O}$ values of purified disc-shaped diatoms were $+40.0\text{‰} \pm 0.2\text{‰}$ (1σ) (MIS 1, $n = 3$), $+41.4\text{‰} \pm 0.2\text{‰}$ (MIS 2, $n = 3$), and $+40.6\text{‰} \pm 0.2\text{‰}$ (MIS 3, $n = 2$) (Figure 5a), showing a reasonable trend for the environmental changes from MIS 3 to MIS 1. The variation of $\delta^{18}\text{O}$ within each sample was $<0.5\text{‰}$. Although the sample number is lower than that of pretreated samples, the standard deviation of the $\delta^{18}\text{O}$ values of the cell sorter-purified samples was smaller than those of the pretreated samples (Figure 5a, Supplemental Table S2). This difference is presumably because of the removal of other types of diatoms and small fragments. The highest $\delta^{18}\text{O}$ value for MIS 2 and the lowest $\delta^{18}\text{O}$ value for MIS 1 are consistent with the environmental changes from MIS 3 to MIS 1. These results indicate the effectiveness and necessity of the purification to obtain accurate $\delta^{18}\text{O}$ records.

Fig. 5

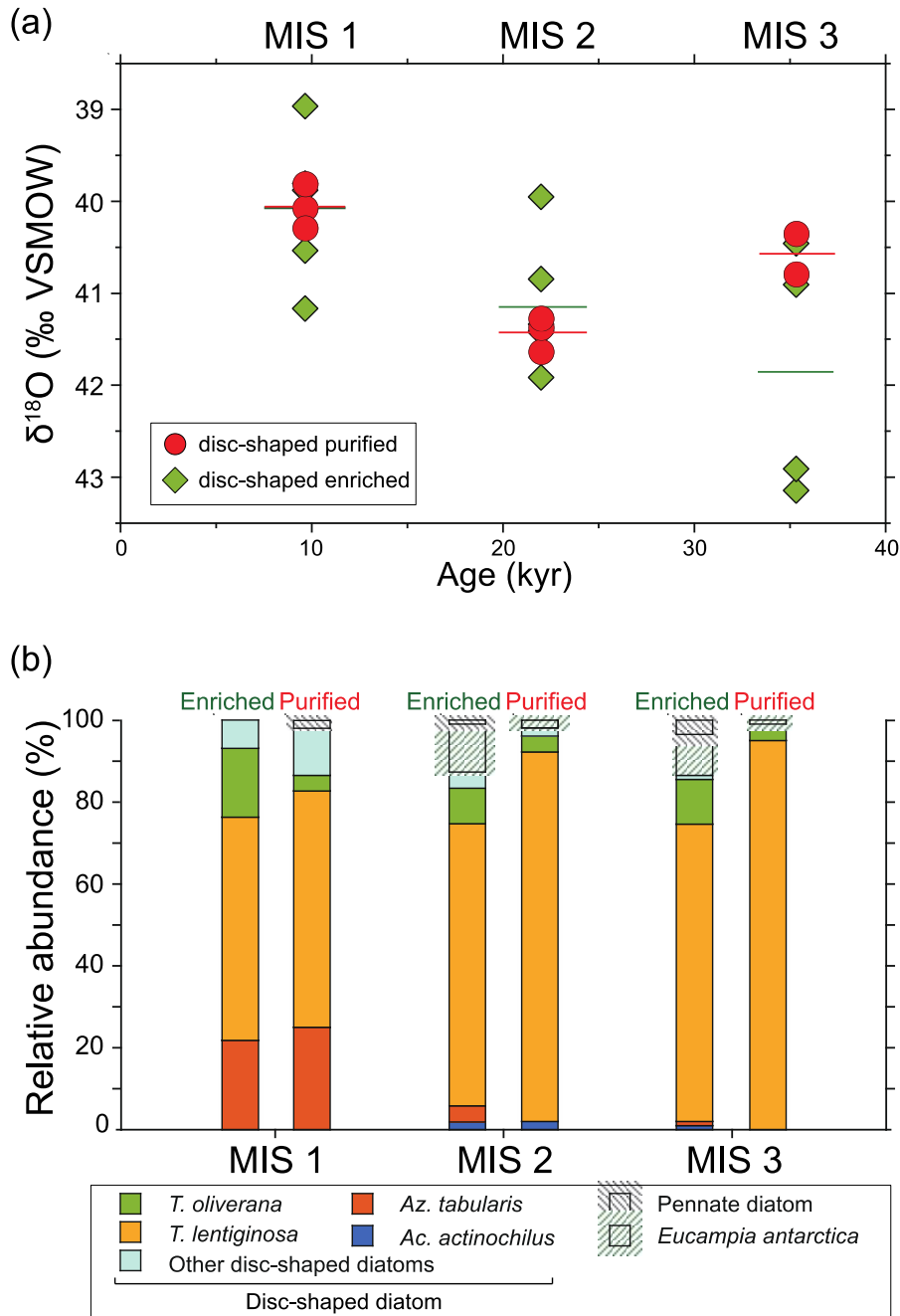


Figure 5. Measured $\delta^{18}\text{O}$ values and species compositions of samples enriched in disc-shaped diatoms by elutriation and purified by cell sorter. (a) Measured $\delta^{18}\text{O}$ values of enriched and purified disc-shaped diatoms from MIS 1–3. (b) Diatom species compositions of enriched and purified disc-shaped-diatom samples from MIS 1–3.

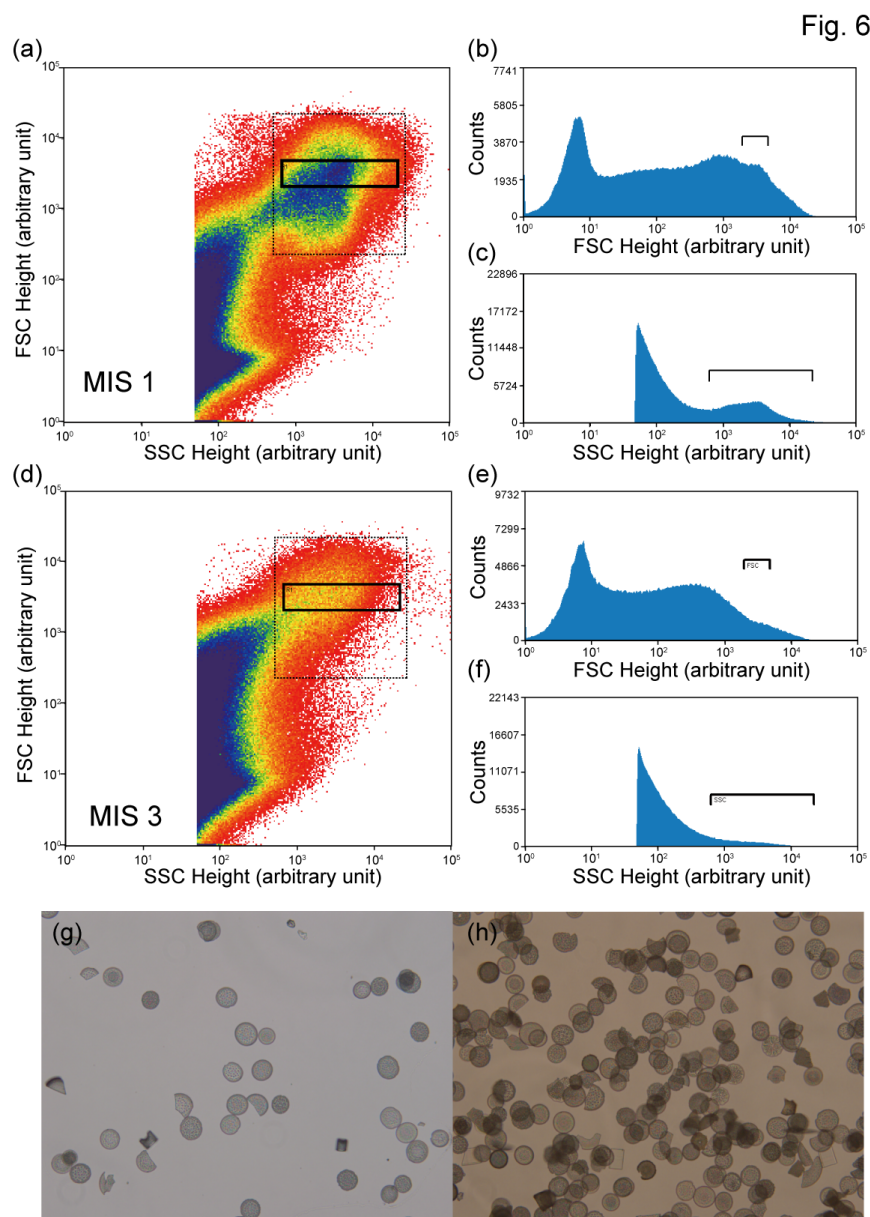


Figure 6. Flow cytograms and photo-micrographs of samples. Plots of (a) FSC height versus SSC height, (b) particle counts versus FSC height, and (c) particle counts versus SSC height for the MIS 1 sample, and (d–f) the same for the MIS 3 sample. Photo-micrographs (g) and (h) show the MIS 3 sample after sorting using the parameters within the dotted and solid squares, respectively, in (d). In (a) and (b), each dot indicates a particle that has passed through the laser. The bluer the color, the more particles there are.

3.4. Variation of $\delta^{18}\text{O}$ in pure disc-shaped diatoms during the last 40 kyr

Using the method established in this study, we analyzed the $\delta^{18}\text{O}$ of purified disc-shaped diatoms ($\delta^{18}\text{O}$ -disc) at 50–100 cm intervals (3–6 kyr) for core COR-1bPC (Figure 7a).

Disc-shaped diatoms comprised more than 95% of the core samples purified for $\delta^{18}\text{O}$ analysis (Figure 7d, Supplemental Table S4). The contents of pennate diatoms were mostly less than 2%, but the sample at 35.4 ka contained 5% of the pennate diatom *Fragilariopsis kerguelensis* (O'Meara) Hustedt, which is the dominant species in the Southern Ocean and indicates open water with no sea-ice cover.^{26,49} The Holocene assemblage of disc-shaped diatoms observed in this study, which is dominated by *T. lentiginosa* (51%–67%) and *Az. tabularis* (16%–28%), is consistent with the previously reported assemblage of disc-shaped diatoms at the Conrad Rise during the Holocene, which contained approximately 63% *T. lentiginosa* and approximately 25% *Az. tabularis*.⁵⁰ These percentages were calculated for disc-shaped diatoms without *Shionodiscus gracilis* var. *gracilis* (Karsten) Alverson, Kang et Theriot (previously known as *Thalassiosira gracilis* var. *gracilis*), which is mostly removed during sieving because of its relatively small size (5–28 μm).⁵¹ This consistency is the evidence that bias was not introduced to the assemblage during the sorting of disc-shaped diatoms by cell sorter.

Although we analyzed only disc-shaped diatoms, the difference in species compositions of the disc-shaped-diatoms would have affected the $\delta^{18}\text{O}$ -disc values because of differences in the timing of production or vital effects for each species. To check the effect of changes in species composition on $\delta^{18}\text{O}$ -disc, we compared $\delta^{18}\text{O}$ -disc to the abundance ratio of *Az. tabularis*, which is abundant in the subantarctic region,⁵² to *T. lentiginosa* (the dominant species in the disc-shaped diatoms), and to the ratio of *T. oliverana*, which is widely distributed in the open-ocean areas of the Southern Ocean,²⁶ to *T. lentiginosa*. There was no clear correlation in these

comparisons, suggesting a negligible effect of species composition changes (Supplemental Figure S2).

The $\delta^{18}\text{O}$ -disc values were compared to the LR04 $\delta^{18}\text{O}$ stack record—which is an average of globally-distributed benthic foraminiferal $\delta^{18}\text{O}$ records—the temperature record in the EPICA Dome C ice core, and the $\delta^{18}\text{O}$ of the planktonic foraminifer *Neogloboquadrina pachyderma* (sinistral) ($\delta^{18}\text{O}$ -Np) and of bulk diatoms ($\delta^{18}\text{O}$ -bulk) during the Holocene at the Conrad Rise, obtained from piston core COR-1PC (54°16'S, 39°46'E; water depth, 2864 m; core length, 408 cm) (Figure 7).^{3,39,43,50}

The $\delta^{18}\text{O}$ -disc profile for core COR-1bPC shows the last glacial cycle since 40 ka (Figure 7a), which can be generally correlated with the LR04 $\delta^{18}\text{O}$ stack record (Figure 7b). During MIS 3, the trend of a gradual increase in $\delta^{18}\text{O}$ -disc from 42.5‰ at 35.4 ka to 43.0‰ at MIS 2 seems to be correlated with the LR04 $\delta^{18}\text{O}$ stack record (Figure 7a, b). In contrast, higher $\delta^{18}\text{O}$ -disc values at 34.4, 36.3, and 38.7 ka compared to those in MIS 2 suggest a lower temperature or higher $\delta^{18}\text{O}$ of seawater at these times than during MIS 2, inconsistent with the LR04 stack curve. It should be noted, however, that the relative abundance of *Actinocyclus actinochilus* (Ehrenberg) Simonsen, which is considered a sea-ice-related species,⁵³ is higher in MIS 3 than MIS 2 (Figure 7d); therefore, the higher $\delta^{18}\text{O}$ -disc may reflect local cooling in the sea-ice zone. Interestingly, *T. oliverana* (an open-ocean species), and even *F. kerguelensis*, indicating open water increased in relative abundance at the $\delta^{18}\text{O}$ local minimum at 35.4 ka, implying a relatively warm, open-ocean environment at that time. These $\delta^{18}\text{O}$ fluctuations during MIS 3, with increases and decreases in open-ocean and sea-ice species, may reflect the expansion and contraction of sea ice associated with the rapid temperature changes recorded in the ice core (Figure 7c), or the seasonality—with winter sea ice and summer open waters. In order to correlate with the ice core

record, analyses with higher time resolution and the construction of accurate age model are required in the future.

At the deglaciation, the decrease of $\delta^{18}\text{O}$ -disc can be correlated with the LR04 $\delta^{18}\text{O}$ stack record. The change of $\delta^{18}\text{O}$ -disc might also be correlated with the temperature record in the EPICA Dome C ice core, although the sampling resolution is low. In particular, the slight increase of $\delta^{18}\text{O}$ -disc at 13.1 ka might correspond to the Antarctic Cold Reversal (Figure 7c); however, the species compositions suggest a warmer environment because this is the period when the warm-water species *Az. tabularis* shows its maximum abundance. Analyses with higher time resolution in future studies should clarify the centennial to millennial environmental changes.

During the Holocene, the relatively low $\delta^{18}\text{O}$ -disc values compared to those before the Holocene are consistent with the LR04 stack record. At the core top presumably corresponding to the present, $\delta^{18}\text{O}$ -disc was analyzed in duplicate, and the averaged value (+38.4‰) shows the lowest value in the core. However, the large variation in $\delta^{18}\text{O}$ -disc during this period cannot be seen in the $\delta^{18}\text{O}$ -Np (Figure 7b).⁵⁰ At the Conrad Rise, there were increases of warm-water diatom species at 9.9–9.3 ka, corresponding to the early Holocene optimum, and periodic spikes in $\delta^{18}\text{O}$ -Np and cold-water diatom taxa after 9.3 ka.⁵⁰ In addition, the maximum percentage of cold water diatoms and a relatively high $\delta^{18}\text{O}$ -Np were observed around 3 ka,⁵⁰ which were attributed to the Antarctic coastal neoglaciation, during which spring sea surface temperature was 1–2 °C lower than during the mid-Holocene.^{50,54} The high $\delta^{18}\text{O}$ -disc peak at 2.7 ka may be suggestive of the temperature decrease during the neoglaciation period. It is possible that $\delta^{18}\text{O}$ -disc reflects the sea surface environment more sensitively than does $\delta^{18}\text{O}$ -Np because the

analyzed disc-shaped diatoms live closer to the sea surface than *N. pachyderma*, which lives in or just below the chlorophyll maximum zone between 50 and 100 m water depth.^{50,55–57}

The $\delta^{18}\text{O}$ -bulk diatom values fluctuated widely between +38‰ and +43‰ (Figure 7a) during the Holocene.⁴³ This variation is greater than that of $\delta^{18}\text{O}$ -disc from the last glacial maximum (LGM) (+43.0‰) to the core top (+38.4‰), suggesting that $\delta^{18}\text{O}$ -bulk does not reflect glacial–interglacial environmental changes. For the $\delta^{18}\text{O}$ -bulk analysis, there was no SPT separation to remove contaminants. Thus, such large variation of $\delta^{18}\text{O}$ -bulk was probably caused by contamination, which potentially increased $\delta^{18}\text{O}$ values as observed in our pretreatment experiment, and by the variety of species of diatom in the samples, including disc-shaped and pennate forms. The difference between $\delta^{18}\text{O}$ -disc and $\delta^{18}\text{O}$ -bulk highlights the effectiveness of our method for purifying disc-shaped diatoms to obtain a more accurate $\delta^{18}\text{O}$ record.

Fig. 7

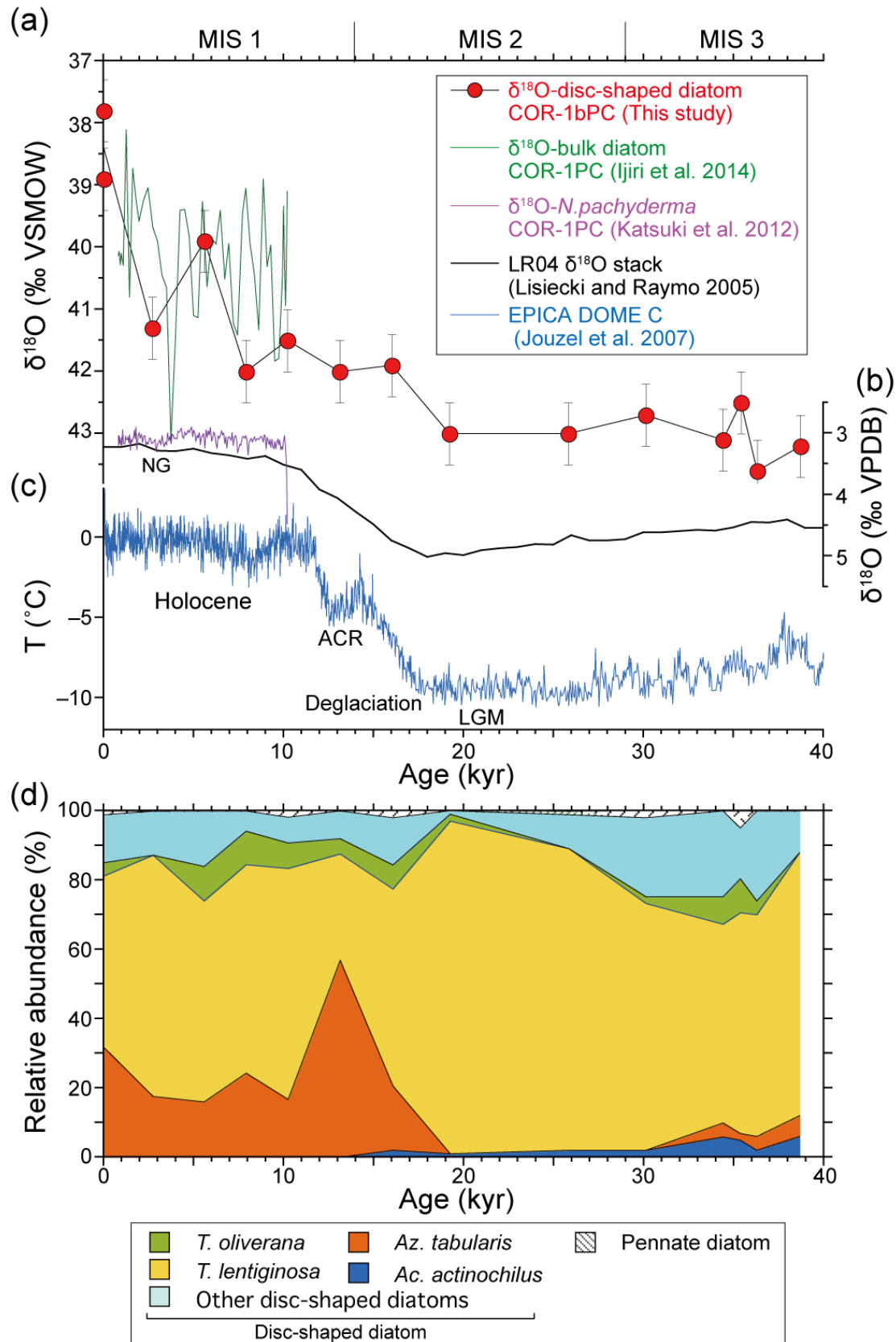


Figure 7. The $\delta^{18}\text{O}$ profile of purified disc-shaped diatoms ($\delta^{18}\text{O}$ -disc) and their species compositions in core COR-1bPC, along with other paleoenvironmental proxies. (a) Measured $\delta^{18}\text{O}$ values of disc-shaped diatoms in core COR-1bPC (red circles) and of bulk diatoms in core COR-1PC (green line), (b) $\delta^{18}\text{O}$ of *N. pachyderma* in core COR-1PC (purple line) and the LR04 $\delta^{18}\text{O}$ stack record (black line), (c) the temperature record in the EPICA Dome C ice core (blue line), and (d) species composition of the samples of purified disc-shaped diatoms from core COR-1bPC. The vertical bars on (a) indicate the boundaries between MIS 1, MIS 2, and MIS 3. NG: neoglaciation; ACR: Antarctic Cold Reversal; LGM: Last Glacial Maximum.

3.5. Assumed oxygen isotope fractionation between water and diatoms

There is a variety of proposed values for oxygen isotope fractionation between water and diatom silica during silica formation based on calibration studies with marine and freshwater diatoms. The reported change in $\delta^{18}\text{O}$ per degree centigrade (i.e., the temperature coefficient) ranges from $-0.19\text{‰}/^{\circ}\text{C}$ to $-0.49\text{‰}/^{\circ}\text{C}$.^{8–10,15,58–60} The temperature coefficient for $\delta^{18}\text{O}$ -disc is unknown, but the change in $\delta^{18}\text{O}$ -disc from the LGM to the present (core top) in core COR-1bPC could constrain the temperature coefficient for disc-shaped diatoms in the Southern Ocean. The difference between the core top ($+38.4\text{‰}$) and the LGM ($+43.0\text{‰}$) is 4.6‰ . Subtracting the global ice volume effects, by which the $\delta^{18}\text{O}$ of seawater ($\delta^{18}\text{O}$ -sw) increased globally by 1.0‰ during the LGM,^{61,62} the remaining 3.6‰ would be due to regional changes in temperature and $\delta^{18}\text{O}$ -sw. The sea surface temperature and $\delta^{18}\text{O}$ -sw over the Conrad Rise observed during research cruises KH-10-7 and KH-16-1 by R/V *Hakuho Maru* during December 2010 (early summer) and February 2016 (late summer) ranged from -0.4 to $+3.9$ $^{\circ}\text{C}$, and from -0.2‰ to 0‰ , respectively (Supplemental Table S5). Applying the temperature coefficient of $-0.2\text{‰}/^{\circ}\text{C}$ derived from diatoms living in a freshwater lake,⁶⁰ the 3.6‰ increase is equivalent to a temperature decrease of 18 $^{\circ}\text{C}$. Subtracting this decrease from the modern-day temperature, the temperature at the LGM is estimated at -14.1 to -18.4 $^{\circ}\text{C}$. This temperature is unlikely because it is significantly below the freezing temperature of seawater (around -2 $^{\circ}\text{C}$). If the temperature at the LGM was -2°C , the increase of $\delta^{18}\text{O}$ by the temperature decrease is 0.3 to 1.2‰ , and that by the local change in $\delta^{18}\text{O}$ -sw is 2.4 to 3.3‰ . Such large change in $\delta^{18}\text{O}$ -sw is also unlikely. If instead we use the maximum temperature coefficient of $-0.49\text{‰}/^{\circ}\text{C}$ deduced from the low temperature (<4 $^{\circ}\text{C}$) data points from the Southern Ocean,¹⁰ the 3.6‰ increase is equivalent to a 7.3 $^{\circ}\text{C}$ decrease. Using this value, the temperature at the LGM is estimated to be from -7.7 to

−3.4 °C; that is, still a few degrees below the freezing temperature. To raise the temperature estimate to above −2 °C, it is necessary to increase the local change in $\delta^{18}\text{O}_{\text{sw}}$ by at least 0.6‰ or the modern temperature by 1.4 °C; both of these are plausible. For now, the temperature coefficient of −0.49‰/°C proposed for high-latitude areas is presumed to be the most applicable.¹⁰

Another possibility for the $\delta^{18}\text{O}$ difference between the core top and the LGM is ^{18}O enrichment of sedimentary silica associated with a decrease in the number of Si–OH groups and the formation of Si–O–Si linkages during silica maturation in sediments.^{63–65} The low $\delta^{18}\text{O}_{\text{disc}}$ at the core top and the rapid increase below could reflect secondary $\delta^{18}\text{O}$ changes by this maturation. At present, the implication of these exchanges and the extent to which silica maturation affects the use of diatom $\delta^{18}\text{O}$ in paleoenvironmental reconstructions remain unknown.¹⁵ We believe that our diatom purification method can contribute to the evaluation of the secondary isotopic change during maturation as well as calibration of the temperature coefficient for specific species.

3.6. Implications for purification of pennate diatoms

It is technically possible to purify pennate diatoms by using cell sorter. The purification of pennate diatoms would be valuable, considering that isotope records from carbonates are uncommon in polar waters due to minimal carbonates, and that in higher latitude cores, pennate diatoms - whether *F. kerguelensis* or sea-ice associated *Fragilariopsis*, are most common.^{26,53} In our method, the elutriation step for the enrichment of disc-shaped diatoms leaves pennate diatoms in the supernatant. However, this supernatant includes not only the pennate diatoms but also many disc-shaped diatoms and silicoflagellates (Supplemental Figure S3). So, if we can find

the area of pennate diatoms in the FSC and SSC plots, with further optimization of elutriation to enrich them, they could then be sorted as well as the disc-shaped diatoms.

4. CONCLUSIONS

We established a new method for purifying disc-shaped diatom frustules from sediment samples using multiple steps of pre-treatments and finally selective sorting by cell sorter and succeeded in almost eliminating clay-mineral contamination and improving the accuracy of $\delta^{18}\text{O}$ measurements of the diatoms. To develop the method, we used samples from a sediment core retrieved from the southwestern slope of the Conrad Rise in the Indian Ocean sector of the Southern Ocean. By using the pretreatments including elutriation—which can enrich the disc-shaped diatoms—we were able to reduce clay-mineral contamination to below 2% for the samples from MIS 2 and MIS 3. There was no significant clay-mineral contamination in the MIS 1 sample, but other contaminants, such as silicoflagellates, potentially increased the $\delta^{18}\text{O}$ values. These other contaminants were also removed by the pretreatments.

The pre-enriched disc-shaped diatoms were further purified by cell sorter. This method can generate samples with more than 95% purity of disc-shaped diatoms regardless of differences in the diatom assemblage and the sediment type of the core sample. The high precision of the method is evident in the standard deviation of $\delta^{18}\text{O}$ -disc in samples purified from the same sediment samples ($\pm 0.2\text{‰}$ [1σ], $n = 3$).

The profile for $\delta^{18}\text{O}$ -disc in core COR-1bPC obtained by this method reflects the last glacial cycle since 40 ka, and can be correlated with the LR04 $\delta^{18}\text{O}$ stack record or the temperature record in the EPICA Dome C ice core, indicating that the method can contribute to obtaining an accurate $\delta^{18}\text{O}$ record of diatoms associated with glacial–interglacial cycles.

ASSOCIATED CONTENT

Supporting information

Scanning electron microscope (SEM) images of diatom frustules before ultrasonification, and after ultrasonification (Figure S1); Measured $\delta^{18}\text{O}$ values of purified disc-shaped diatoms ($\delta^{18}\text{O}$ -disc) versus the abundance ratios of *Azpeitia tabularis*:*Thalassiosira lentiginosa*, and the *Thalassiosira oliverana*:*T. lentiginosa* (Figure S2); SEM image of the floating, pennate-diatom-rich fraction of the MIS 1 sample after elutriation (Figure S3) (PDF).

Raw data for the purification of disc-shaped diatoms (Table S1–S5)(Excel).

AUTHOR INFORMATION

Corresponding Author

Akira Ijiri. Kochi Institute for Core Sample Research (KOCHII), Institute for Extra-cutting-edge Science and Technology Avant-garde Research (X-Star), Japan Agency for Marine-Earth Science and Technology (JAMSTEC), B200 Monobe, Nankoku, Kochi 783-8502, Japan

Graduate School of Maritime Sciences, Kobe University, 5-1-1 Fukaeminamimachi, Higashinada-ku, Kobe 658-0022, Japan

Email: ijiri@maritime.kobe-u.ac.jp

Authors

Takeshi Izumi. Graduate School of Integrated Arts and Sciences, Kochi University, 2-5-1 Akebono-cho, Kochi 780-8520, Japan

Yuki Morono. Kochi Institute for Core Sample Research (KOCHII), Institute for Extra-cutting-edge Science and Technology Avant-garde Research (X-Star), Japan Agency for Marine-Earth Science and Technology (JAMSTEC), B200 Monobe, Nankoku, Kochi 783-8502, Japan

Yuji Kato. Center for Advanced Marine Core Research, Kochi University, B200 Monobe, Nankoku, Kochi 783-8502, Japan

Takeshi Terada. Marine Works Japan Ltd., 3-54-1 Oppamahigashimachi, Yokosuka 237-0063, Japan

Minoru Ikehara. Center for Advanced Marine Core Research, Kochi University, B200 Monobe, Nankoku, Kochi 783-8502, Japan

Author Contributions

All authors have given approval to the final version of the manuscript.

Funding Sources

This work was supported by JSPS KAKENHI Grant Numbers 23244102, 17H06318.

ACKNOWLEDGMENT

We acknowledge the officers, crew, and scientific party of cruise KH-10-7 of R/V *Hakuho Maru* for sample retrieval and technical support. We thank Dr. M. Yamane and Dr. G. Uramoto for their technical advice on sample preparation. We also thank Dr. Katsuki for providing the raw count data of diatoms. The authors are grateful to M. Odani for technical assistance.

ABBREVIATIONS

ACC, Antarctic Circumpolar Current; CF-IRMS, continuous-flow isotope ratio mass spectrometry; CO, carbon monoxide; $\delta^{13}\text{C}$, carbon isotopic composition; $\delta^{15}\text{N}$, nitrogen isotopic composition; $\delta^{18}\text{O}$, oxygen isotopic composition; $\delta^{30}\text{Si}$, silicon isotopic composition; EDS, Energy-dispersive X-ray spectroscopy; FSC, forward scatter; iHTR, inductive high-temperature carbon reduction; JAMSTEC, Japan Agency for Marine-Earth Science and Technology; KOCHII, Kochi Institute for Core Sample Research; LGM, Last Glacial Maximum; MIS, Marine Isotope Stage; SEM, Scanning Electron Microscope; SPT, sodium polytungstate; SSC, side scatter; X-Star, Institute for Extra-cutting-edge Science and Technology Avant-garde Research

REFERENCES

- (1) Emiliani, C. Pleistocene temperatures. *J. Geol.* **1955**, *63*, 538–578.
- (2) Shackleton, N. Depth of pelagic foraminifera and isotopic changes in Pleistocene oceans. *Nature* **1968**, *218*, 79–80.
- (3) Lisiecki, L. E.; Raymo, M. E. A Pliocene-Pleistocene stack of 57 globally distributed benthic $\delta^{18}\text{O}$ records, *Paleoceanography*, **2005**, *20*, PA1003, DOI:10.1029/2004PA001071.

- (4) Dutkiewicz, A.; O’Callaghan, S.; Müller, R. D. Controls on the distribution of deep-sea sediments. *Geochemistry, Geophys. Geosystems*, **2016**, *17*, 3075–3098.
- (5) Martin, J. H. Glacial-interglacial CO₂ change: The iron hypothesis. *Paleoceanography*, **1990**, *5*, 1–13, DOI:10.1029/PA005i001p00001.
- (6) Ikehara, M.; Kawamura, K.; Ohkouchi, N.; Murayama, M.; Nakamura, T.; Taira, A. Variations of terrestrial input and marine productivity in the Southern Ocean (48° S) during the last two deglaciations. *Paleoceanography*, **2000** *15*, 170–180, DOI:10.1006/qres.2001.2252.
- (7) Sigman, D. M.; Jaccard, S. L.; Haug, G. H. Polar ocean stratification in a cold climate. *Nature*, **2004**, *428*, 59–63, DOI:10.1038/nature02357.
- (8) Labeyrie, L. D. New approach to surface seawater paleotemperatures using 18O/16O ratios in silica of diatom frustules. *Nature*, **1974**, *248*, 40–42.
- (9) Juillet-Leclerc, A.; Labeyrie, L. Temperature dependence of the oxygen isotopic fractionation between diatom silica and water. *Earth Planet. Sci. Lett.* **1987**, *84*, 69–74, DOI:10.1016/0012-821X(87)90177-4.
- (10) Shemesh, A.; Charles, C. D.; Fairbanks, R. G. Oxygen isotopes in biogenic silica: global changes in ocean temperature and isotopic composition. *Science*, **1992**, *256*, 1434–1436, DOI:10.1126/science.256.5062.1434.
- (11) Shemesh, A.; Burckle, L. H.; Hays, J. D. Late Pleistocene oxygen isotope records of biogenic silica from the Atlantic sector of the Southern Ocean. *Paleoceanography*, **1995**, *10*, 179–196, DOI:10.1029/94PA03060.

- (12) Shemesh, A.; Hodell, D.; Crosta, C.; Kanfoush, S.; Charles, T.; Guilderson, T. Sequence of events during the last deglaciation in Southern Ocean sediments and Antarctic ice cores. *Paleoceanography*, **2002**, *17*, 1056, DOI:10.1029/2000PA000599.
- (13) Hodell, D. A.; Kanfoush, S. L.; Shemesh, A.; Crosta, X.; Charles, C. D.; Guilderson, T. P.; Abrupt Cooling of Antarctic Surface Waters and Sea Ice Expansion in the South Atlantic Sector of the Southern Ocean at 5000 cal yr B.P. *Quat. Res.*, **2001**, *56*, 191–198, DOI:10.1006/qres.2001.2252.
- (14) Swann, G. E. A.; Maslin, M. A.; Leng, M. J.; Sloane, H. J.; Haug, G. H. Diatom $\delta^{18}\text{O}$ evidence for the development of the modern halocline system in the subarctic northwest Pacific at the onset of major Northern Hemisphere glaciation. *Paleoceanography*, **2006**, *21*, PA1009, DOI:10.1029/2005PA001147.
- (15) Swann, G. E. A.; Leng, M. J. A review of diatom $\delta^{18}\text{O}$ in palaeoceanography. *Quat. Sci. Rev.*, **2009**, *28*, 384–398, ^[1]_{SEP} DOI:10.1016/j.quascirev.2008.11.002.
- (16) Morley, D. W.; Leng, M. J.; Mackay, A. W.; Sloane, H. J.; Rioual, P.; Battarbee, R. W. Cleaning of lake sediment samples for diatom oxygen isotope analysis. *J. Paleolimnol.*, **2004**, *31*, 391–401.
- (17) Giddings, J. C. A System Based on Split-Flow Lateral-Transport Thin (SPLITT) Separation Cells for Rapid and Continuous Particle Fractionation. *Sep. Sci. Technol.*, **1985**, *20*, 749–768, DOI:10.1080/01496398508060702.

- (18) Rings, A.; Lücke, A.; Schleser, G. H. A new method for the quantitative separation of diatom frustules from lake sediment. *Limnol. Oceanogr. Methods*, **2004**, 2, 25–34, DOI:10.4319/lom.2004.2.25.
- (19) Leng, M. J.; Barker, P. A. A review of the oxygen isotope composition of lacustrine diatom silica for paleoclimate reconstruction. *Earth Sci. Rev.*, **2006**, 75, 5–27, DOI:10.1016/j.earscirev.2005.10.001.
- (20) Tennant, R. K.; Richard, T. J.; Love, J.; Lee, R. A new flow cytometry method enabling rapid purification of diatoms from silica-rich lacustrine sediments. *J. Paleolimnol.*, **2013**, 49, 305–309.
- (21) Swann, G. E. A.; Leng, M. J.; Sloane, H. J.; Maslin, M. A.; Onodera, J. Diatom oxygen isotopes: evidence of a species effect in the sediment record. *Geochemistry, Geophys. Geosystems*, **2007**, 8, Q06012, DOI:10.1029/2006GC001535.
- (22) Swann, G.E.A.; Leng, M. J.; Sloane, H. J.; Maslin, M. A. Isotope offsets in marine diatom $\delta^{18}\text{O}$ over the last 200 ka. *J. Quat. Sci.*, **2008**, 23, 389–400, DOI:10.1002/jqs.1185.
- (23) Studer, A. S.; Sigman, D. M.; Martínez-García, A.; Benz, V.; Winckler, G.; Kuhn, G.; Esper, O.; Lamy, F.; Jaccard, S. L.; Wacker, L.; Oleynik, S.; Gersonde, R.; Haug, G. H. Antarctic Zone nutrient conditions during the last two glacial cycles. *Paleoceanography*, **2015**, 30, 845–862, DOI:10.1002/2014PA002745.
- (24) Morono, Y.; Terada, T.; Kallmeyer, J.; Inagaki, F. An improved cell separation technique for marine subsurface sediments: applications for high-throughput analysis using flow

cytometry and cell sorting. *Environ. Microbiol. Rep.*, **2013**, *15*, 2841–2849, DOI:10.1111/1462-2920.12153.

(25) Uramoto, G.; Morono, Y.; Tomioka, N.; Wakaki, S.; Nakada, R.; Wagai, R.; Uesugi, K.; Takeuchi, A.; Hoshino, M.; Suzuki, Y.; Shiraishi, F.; Mitsunobu, S.; Suga, H.; Takeichi, Y.; Takahashi, Y.; Inagaki, F. Significant contribution of subseafloor microparticles to the global manganese budget. *Nat. Commun.*, **2019**, *10*, 1–10, DOI:10.1038/s41467-019-08347-2.

(26) Crosta, X.; Romero, O.; Armand, L. K.; Pichon, J.-J. The biogeography of major diatom taxa in Southern Ocean sediments: 2. Open ocean related species. *Palaeogeogr. Palaeoclimatol. Palaeoecol.*, **2005**, *223*, 66–92. DOI:10.1016/j.palaeo.2005.03.028.

(27) Cody, R. D.; Levy, R. H.; Harwood, D. M.; Sadler, P. M. Thinking outside the zone: High-resolution quantitative diatom biochronology for the Antarctic Neogene. *Palaeogeogr. Palaeoclimatol. Palaeoecol.* **2008**, *260*, 92–121, DOI:10.1016/j.palaeo.2007.08.020.

(28) Crosta, X.; Pichon, J.-J.; Burckle, L. H. Application of modern analog technique to marine Antarctic diatoms: reconstruction of maximum sea-ice extent at the Last Glacial Maximum. *Paleoceanography*, **1998**, *13*, 286–297, DOI:10.1029/98PA00339.

(29) De la Rocha, C. L.; Brzezinski, M. A.; DeNiro, M. J.; Shemesh, A. Silicon-isotope composition of diatoms as an indicator of past oceanic change. *Nature*, **1998**, *395*, 680–683, DOI:10.1038/27174.

(30) De la Rocha, C. L. Opal-based isotopic proxies of paleoenvironmental conditions. *Global Biogeochem. Cycles*, **2006**, *20*, GB4S09. DOI:10.1029/2005GB002664.

(31) Reynolds, B. C.; Frank, M.; Halliday, A. N. Evidence for a major change in silicon cycling in the subarctic North Pacific a 2.73 Ma. *Paleoceanography*, **2008**, *23*, PA4219, DOI:10.1029/2007PA001563.

(32) Maier, E.; Chaplign, B.; Abelmann, A.; Gersonde, R.; Esper, O.; Ren, J.; Friedrichsen, H.; Meyer, H.; Tiedemann, R. Combined oxygen and silicon isotope analysis of diatom silica from a deglacial subarctic Pacific record. *J. Quat. Sci.*, **2013**, *28*, 571–581, DOI:10.1002/jqs.2649.

(33) Singer, A. J.; Shemesh, A. Climatically linked carbon isotope variation during the past 430,000 years in Southern Ocean sediments. *Paleoceanography*, **1995**, *10*, 171–177, DOI:10.1029/94PA03319.

(34) Sigman, D. M.; Altabet, M. A.; Francois, R.; McCorkle, D. C.; Gaillard, J.-F. The isotopic composition of diatom-bound nitrogen in Southern Ocean sediments. *Paleoceanography*, **1999**, *14*, 118–134, DOI:10.1029/1998PA900018.

(35) Crosta, X.; Shemesh, A. Reconciling down core anticorrelation of diatom carbon and nitrogen isotopic ratios from the Southern Ocean. *Paleoceanography*, **2002**, *17*, 1010, DOI:10.1029/2000PA000565.

(36) Schneider-Mor. A.; Yam, R.; Bianchi, C.; Kunz-Pirrung, M.; Gersonde, R.; Shemesh, A. Diatom stable isotopes, sea presence and sea surface temperature records of the past 640 ka in the Atlantic sector of the Southern Ocean. *Geophys. Res. Lett.*, **2005**, *32*, L10704, DOI:10.1029/2005GL022543.

(37) Oiwane, H.; Ikehara, M.; Suganuma, Y.; Miura, H.; Nakamura, Y.; Sato, T.; Nogi, Y.; Yamane, M.; Yokoyama, Y. Sediment waves on the Conrad Rise, Southern Ocean: Implications for the migration history of the Antarctic Circumpolar Current. *Mar. Geol.*, **2014**, *348*, 27–36, DOI:10.1016/j.margeo.2013.10.008.

(38) Ansorge, I. J.; Roman, R.; Durgadoo, J. V.; Ryan, P. G.; Dlamini, L.; Gebhardt, Z.; Rainier, S.; Smith, M.; Mtonsti, T.; Lutjeharms, J. R. E. The first oceanographic survey of the Conrad Rise. *S. Afr.*, **2008**, *104*, 333–336.

(39) Jouzel, J.; Masson-Delmotte, V.; Cattani, O.; Dreyfus, G.; Falourd, S.; Hoffmann, G.; Minster, B.; Nouet, J.; Barnola, J. M.; Chappellaz, J.; Fischer, H.; Gallet, J. C.; Johnsen, S.; Leuenberger, M.; Loulergue, L.; Luethi, D.; Oerter, H.; Parrenin, F.; Raisbeck, G.; Raynaud, D.; Schilt, A.; Schwander, J.; Selmo, E.; Souchez, R.; Spahni, R.; Stauffer, B.; Steffensen, J. P.; Stenni, B.; Stocker, T. F.; Tison, J. L.; Werner, M.; Wolff, E. W. Orbital and millennial Antarctic climate variability over the past 800,000 years. *Science*, **2007**, *317*, 793–796, DOI:10.1126/science.1141038.

(40) Shukla, S. K.; Crespin, J.; Crosta, X. *Thalassiosira lentiginosa* size variation and associated biogenic silica burial in the Southern Ocean over the last 42 kyrs. *Mar. Micropaleontol.*, **2016**, *127*, 74–85, DOI:10.1016/j.marmicro.2016.07.006.

(41) Munsterman, D.; Kerstholt, S. Sodium polytungstate, a new non-toxic alternative to bromoform in heavy liquid separation. *Rev. Palaeobot. Palynol.*, **1996**, *91*, 417–422.

(42) Lücke, A.; Moschen, R.; Schleser, G. H. High temperature carbon reduction of silica: a novel approach for oxygen isotope analysis of biogenic opal. *Geochim. Cosmochim. Acta*, **2005**, *69*, 1423–1433, DOI:10.1016/j.gca.2004.09.022.

- (43) Ijiri, A.; Yamane, M.; Ikehara, M.; Yokoyama, Y.; Okazaki, Y. Online oxygen isotope analysis of submilligram quantities of biogenic opal using the inductive high-temperature carbon reduction method coupled with continuous-flow isotope ratio mass spectrometry. *J. Quat. Sci.*, **2014**, 29, 455–462, DOI:10.1002/jqs.2716.
- (44) Chaplignin, B.; Leng, M. J.; Webb, E.; Alexandre, A.; Dodd, J. P.; Ijiri, A.; Lücke, A.; Shemesh, A.; Abelman, A.; Herzsuh, U.; Longstaffe, F. J.; Meyer, H.; Moschen, R.; Okazaki, Y.; Rees, N. H.; Sharp, Z. D.; Sloane, H. J.; Sonzogni, C.; Swann, G. E. A.; Sylvestre, F.; Tyler, J. J.; Yam, R. Inter-laboratory comparison of oxygen isotope compositions from biogenic silica. *Geochim. Cosmochim. Acta*, **2011**, 75, 7242–7256. DOI:10.1016/j.gca.2011.08.011.
- (45) Brewer, T. S.; Leng, M. J.; Mackay, A. W.; Lamb, A. L.; Tyler, J. J.; Marsh, N. G. Unravelling contamination signals in biogenic silica oxygen isotope composition: the role of major and trace element geochemistry. *J. Quat. Sci.*, **2008**, 23, 321–330, DOI:10.1002/jqs.1171.
- (46) Chaplignin, B.; Meyer, H.; Bryan, A.; Snyder, J.; Kemnitz, H. Assessment of purification and contamination correction methods for analysing the oxygen isotope composition from biogenic silica. *Chem. Geol.*, **2012**, 300–301, 185–199, DOI:10.1016/j.chemgeo.2012.01.004.
- (47) Savin, S. M.; Epstein, S. The oxygen and hydrogen isotope geochemistry of clay minerals. *Geochim. Cosmochim. Acta*, **1970**, 34, 25–42, DOI:10.1016/0016-7037(70)90149-3.
- (48) Suček, R. K.; Land, L. S. Isotopic geochemistry of burial-metamorphosed volcanogenic sediments, great valley sequence, Northern California. *Geochim. Cosmochim. Acta*, **1983**, 47, 1487–1499. DOI:10.1016/0016-7037(83)90308-3.

- (49) Abelmann, A.; Gersonde, R.; Cortese, G.; Kuhn, G.; Smetacek, V. Extensive phytoplankton blooms in the Atlantic sector of the glacial Southern Ocean. *Paleoceanography*, **2006**, *21*, PA1013, DOI:10.1029/2005PA001199.
- (50) Katsuki, K.; Ikehara, M.; Yokoyama, Y.; Yamane, M.; Khim, B. K. Holocene migration of oceanic front systems over the Conrad Rise in the Indian Sector of the Southern Ocean. *J. Quat. Sci.*, **2012**, *27*, 203–210, DOI:10.1002/jqs.1535.
- (51) Hasle, G. R.; Syvertsen, E. E. Marine diatoms. In: *Identifying Marine Diatoms and Dinoflagellates*. Tomas, C. R. Ed: Academic Press, San Diego; **1997**.
- (52) Romero, O. E.; Armand, L. K.; Crosta, X.; Pichon, J.-J. The biogeography of major diatom taxa in Southern Ocean surface sediments: 3. Tropical/subtropical species. *Palaeogeogr. Palaeoclimatol. Palaeoecol.*, **2005**, *223*, 49–65, DOI:10.1016/j.palaeo.2005.03.027.
- (53) Armand, L. K., Crosta, X., Romero, O., Pichon, J.-J. The biogeography of major diatom taxa in Southern Ocean sediments: 1. Sea ice related species. *Palaeogeogr. Palaeoclimatol. Palaeoecol.*, **2005**, *223*, 93–126, DOI:10.1016/j.palaeo.2005.02.015.
- (54) Crosta, X.; Denis, D.; Ther, O. Sea ice seasonality during the Holocene, Adélie Land, East Antarctica. *Mar. Micropaleontol.*, **2008**, *66*, 222–232, DOI:10.1016/j.marmicro.2007.10.001
- (55) Quéguiner, B. Iron fertilization and the structure of planktonic communities in high nutrient regions of the Southern Ocean. *Deep Sea Res. Part II*, **2013**, *90*, 43–54, DOI: 10.1016/j.dsr2.2012.07.024.
- (56) Bathmann, U. V.; Scharek, R.; Klaas, C.; Dubischar, C. D.; Smetacek, V. Spring development of phytoplankton biomass and composition in major water masses of the Atlantic

sector of the Southern Ocean. *Deep Sea Res. Part II*, **1997**, 44, 51–67, DOI:10.1016/S0967-0645(96)00063-X.

(57) Bergami, C.; Capotondia, L.; Langonea, L.; Giglio, F.; Ravaioli, M. Distribution of living planktonic foraminifera in the Ross Sea and the Pacific sector of the Southern Ocean (Antarctica). *Mar. Micropaleontol.*, **2009**, 73, 37–48, DOI:10.1016/j.marmicro.2009.06.007.

(58) Matheney, R. K.; Knauth, L. P. Oxygen-isotope fractionation between marine biogenic silica and seawater, *Geochim. Cosmochim. Acta*, **1989**, 53, 3207–3214, DOI:10.1016/0016-7037(89)90101-4.

(59) Brandriss, M. E.; O’Neil, J. R.; Edlund, M. B.; Stoermer, E. F. Oxygen isotope fractionation between diatomaceous silica and water. *Geochim. Cosmochim. Acta*, **1998**, 62, 1119–1125, DOI:10.1016/S0016-7037(98)00054-4.

(60) Moschen, R.; Lücke, A.; Schleser, G. H. Sensitivity of biogenic silica oxygen isotopes to changes in surface water temperature and palaeoclimatology. *Geophys. Res. Lett.*, **2005**, 32, L07708, DOI:10.1029/2004GL022167.

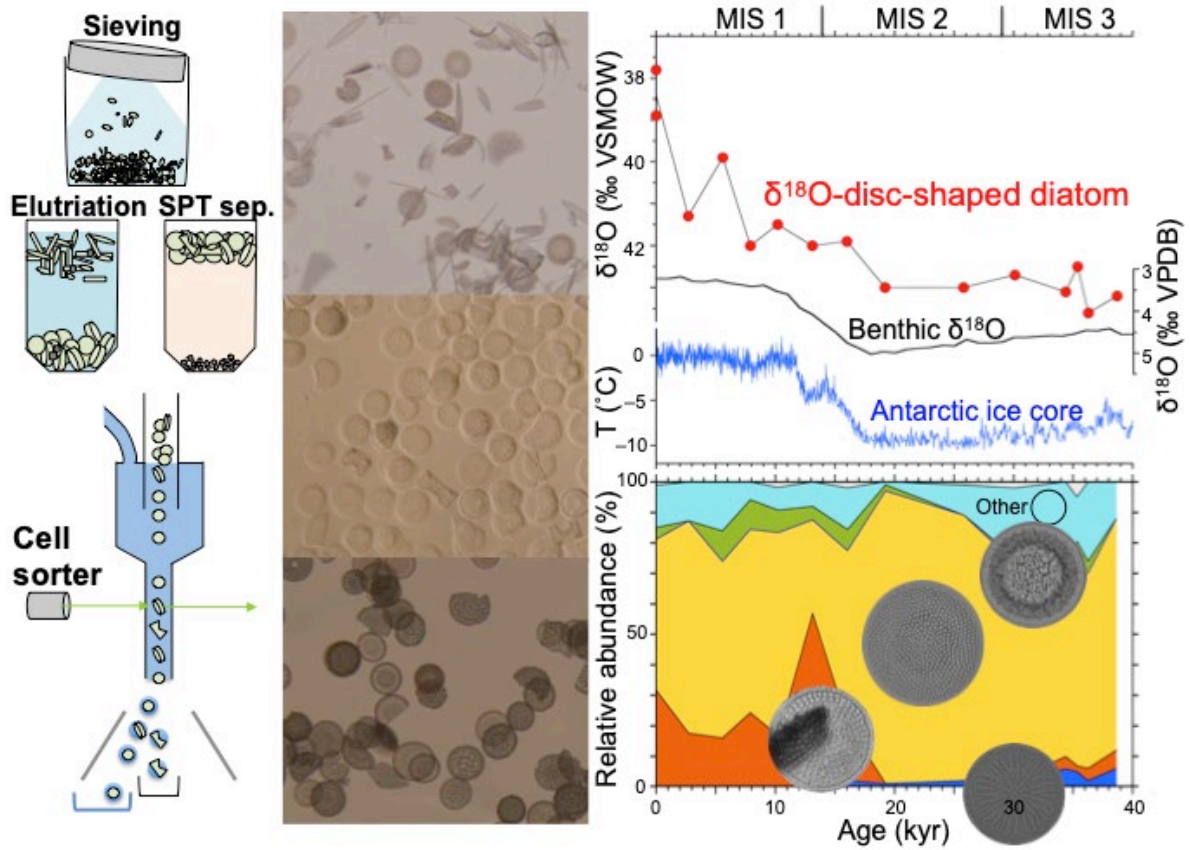
(61) Schrag, D. P.; Hampt, G.; Murray, D. W. Pore fluid constraints on the temperature and oxygen isotopic composition of the glacial ocean. *Science*, **1996**, 272, 1930–1932,^[1]_[SEP] DOI:10.1126/science.272.5270.1930.

(62) Schrag, D. P.; Adkins, J. F.; McIntyre, K.; Alexander, J. L.; Hodell, D. A.; Charles, C. D.; McManus, J. F. The oxygen isotopic composition of seawater during the Last Glacial Maximum. *Quat. Sci. Rev.* **2002**, 21, 331–342 DOI:10.1016/S0277-3791(01)00110-X.

(63) Schmidt, M.; Botz, R.; Stoeffer, P.; Anders, T.; Bohrmann, B. Oxygen isotopes in marine diatoms: A comparative study of analytical techniques and new results on the isotope composition of recent marine diatoms. *Geochim. Cosmochim. Acta*, **1997**, *61*, 2275–2280, DOI:10.1016/S0016-7037(97)00081-1.

(64) Schmidt, M.; Botz, R.; Rickert, D.; Bohrmann, G.; Hall, S. R.; Mann, S. Oxygen isotopes of marine diatoms and relation to opal-A maturation, *Geochim. Cosmochim. Acta*, **2001**, *65*, 201–211, DOI:10.1016/S0016-7037(00)00534-2.

(65) Moschen, R.; Lücke, A.; Parplies, J.; Radtke, U.; Schleser, G. H. Transfer and early diagenesis of biogenic silica oxygen isotope signals during settling and sedimentation of diatoms in a temperate freshwater lake (Lake Holzmaar, Germany). *Geochim. Cosmochim. Acta*, **2006**, *70*, 4367–4379, DOI:10.1016/j.gca.2006.07.001.



For Table of Contents Only